

INTERACTIVE BEAM TUNING SIMULATOR FOR THE SLC FINAL FOCUS*

W. T. FORD

Department of Physics, University of Colorado, Boulder, CO 80309-0390

W. KOZANECKI AND T. LOHSE

Stanford Linear Accelerator Center, Stanford University, Stanford, CA 94309

R. V. SERVRANCKX

Accelerator Laboratory, University of Saskatchewan, Saskatoon, Saskatchewan S7N 0W0, CANADA

ABSTRACT

An interface to the DIMAD beam optics computer program enables the operator to perform in simulation the sequence of magnet adjustments that would be used online for tuning the Stanford Linear Collider Final Focus System. The program accepts any input beam matrix from a disk file and presents a menu of magnet adjustments and scan and display options. The results of a ray trace calculation are presented as profiles or envelope plots on the graphics screen. We give results from studies of the optimization of the beam under various input conditions.

1. INTRODUCTION

A number of computer programs (*e.g.*, TRANSPORT,¹ TURTLE,² DIMAD³) are widely used for the design and analysis of magnetic particle beam transport systems. We wanted a simulation program to model the SLC Final Focus System (FFS) that would provide the user with interactive access to the same controls and readback information as the actual beamline (no more and no less), so that we could gain experience with the tuning procedures to optimize our utilization of real beam time. The program (DIMUSR) has proved valuable in a number of ways, including training physicists and operators who participate in the beam commissioning to: (a) explore distortions of the input beam, (b) optimize the operating parameters, (c) check consistency between designed and observed beam characteristics, (d) set up special test configurations; and (e) investigate consequences of modifications of the beamline, its instrumentation or the tuning procedures.

2. PROGRAM STRUCTURE AND OPERATION

With the program DIMAD one can study the motions of particles in circular machines or beam lines. Particle trajectories are computed according to the second-order matrix formalism.¹ The program accepts data records to define the beam line in the MAD standard format⁴ and to compute beam and transport matrices, adjust beam parameters, trace rays, etc. For application to the SLC, both the non-linear and coupled-plane capabilities of this program are essential. The use of ray tracing permits the generation of beam profiles at points corresponding to profile measuring stations in the actual machine.

For the DIMUSR implementation, we made a very minor modification to DIMAD itself, namely, the addition into the MAD input command repertoire of one new command, USERINT, to invoke the interface routine. We start DIMAD with input decks which define the transport system and incoming beam matrix. A USERINT card transfers control to the interface routine. This routine temporarily diverts the input and output streams of DIMAD to scratch files which it sets up or reads back to prepare displays at the interactive terminal.

DIMUSR's interface routine displays a menu at the terminal containing a list of the focusing elements that are adjustable (counterparts of those in the actual machine). Nominal values and menu fields which can accept alterations of these are provided.

The menu also lists the profile monitoring stations in the beam line, together with an option to plot the x - and y projections of the beam envelope along the beam line, with parameters that control the scales of the plots. Any of the scale parameters can be overwritten by the user to override the defaults.

The computer terminal's function keys are assigned to the program's user-invoked functions. Typically the program traces the selected number of rays through the beam line and generates from these a profile at the chosen station. It may first adjust a focusing element, if the element was selected with a non-zero value of its "step" entry. As another option, the user may request a set of three profiles, corresponding to successive values of the element's focusing strength centered around the current value (Fig. 1). This option approximates the effect of observing a profile screen in the real machine while adjusting a magnet's strength with a knob. Or the user can select a five-point sweep of a parameter to get plots of the beam x - and y widths and their correlation as functions of the parameter with a parabola fit, as in Fig. 2. The "Accept" key causes the parameter value at the minimum of the parabola to become the new current value for that parameter. Where appropriate, variations can be selected as linear combinations of quadrupole strengths, such as the ones for the final demagnifying triplet that correspond to displacement along the beam line of the horizontal or vertical waist.

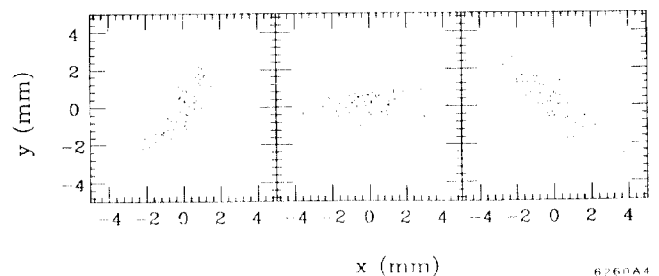


Fig. 1. Profile at the screen ST4, located at a high- β point between the triplets in the final telescope, for three equally-spaced settings of the upstream skew quadrupole SQ17.5.

Certain other procedures that are performed automatically by the control computer in the real machine (see Ref. 5) have analogs in the simulation. A function key on the terminal invokes the computation of the sextupole settings that will minimize chromatic aberrations for the current setting of the quadrupoles. Here, as on the SLC computer, DIMAD minimizes the value of the second-order matrix elements T_{522} and T_{544} for the inverse transport system (interaction point back to the beginning of the FFS).⁶ Similarly, for the dispersion matching we calculate at the touch of a key the correction quadrupole settings that remove the dispersion and its derivative downstream of the matching section. This, of course, is a substantial shortcut compared with what must be done to achieve this in the real beam line.⁷ The betatron angular spread adjustment⁷ could be

* Work supported by the Department of Energy, contracts DE-AC03-76SF00515 and DE-AC02-86ER40253.

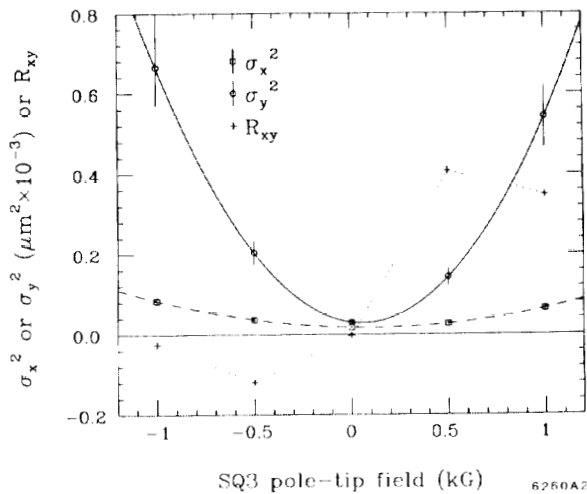


Fig. 2. Projected widths of the profile at the interaction point and their correlation as functions of the setting of the downstream skew quadrupole SQ3.

incorporated as well, but in fact we simulate that process with a separate program (BETAMAT).

A permanent copy of the results at any stage can be saved by requesting the “log” function with a key. Both a graphics image and a printer version of the current display, plus the current menu and some other numerical data, are added to files that will be available after the program is terminated.

3. INFLUENCE OF INPUT BEAM DISTORTIONS

Besides the magnet string specification, DIMUSR accepts an input data file containing the initial beam matrix (*e.g.*, at the end of the linac) and a transport matrix (*e.g.*, representing the arc). We used this facility to study the problem of tuning the FFS with a misaligned arc. Transport matrices were prepared by analyzing the arc model with random alignment perturbations (“seeds”) with TURTLE.⁵ The FFS tuning procedure (see Fig. 4 of Ref. 5) was carried out for several of these arc misalignment seeds. Typically, we found that the spot size at the interaction point (IP) could be adjusted to $\sigma_x^* \approx \sigma_y^* \approx 2 \mu\text{m}$, about 25% larger than for a perfect arc.

Besides the nominal linac emittance of $\epsilon_x = \epsilon_y = 3 \cdot 10^{-10}$ rad m we also ran the seeds with the horizontal emittance increased to $12 \cdot 10^{-10}$ rad m. The issue here was to see what harm might come from unequal emittances in view of the fact that only two skew quad adjustments are available to remove cross-plane coupling. With $\epsilon_x = \epsilon_y$ and the further requirement that we have a waist at the IP, the cross-plane coupling beam matrix correlation coefficients obey the relations⁹

$$\begin{aligned} r_{23} &= r_{14} \quad , \\ r_{24} &= -r_{13} \quad . \end{aligned}$$

These are tested for the simulations by the plots shown in Fig. 3. We see that the conditions relating the pairs are satisfied as expected for an equal emittance input beam (open circle points in

the figure). For unequal input emittances (crosses), they are not. In the tuning procedure, the adjustment of the skew quadrupole SQ17.5 to make an erect beam at the final triplet should produce a small r_{24} , and indeed all the points have $|r_{24}|$ less than 0.3 or so. But for unequal emittances, $|r_{13}|$ is greater than 0.4 for all but one seed, corresponding to profiles at the IP that are tilted if they are not round.

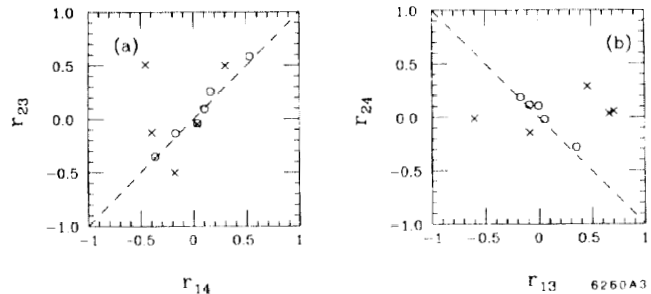


Fig. 3. (a) r_{23} vs r_{14} and (b) r_{24} vs r_{13} for the IP σ matrices for the five seeds. Open circles represent the equal-emittance input beam; crosses, the quadrupled horizontal emittance beam. Dashed lines indicate the relations expected for equal emittances.

The consequence of these effects is that the best spots we could achieve with the larger ϵ_x were about $3.3 \mu\text{m}$ in either plane. The perturbed arc introduces cross-plane coupling that feeds the larger horizontal emittance into the vertical. The spot degradation comes from a combination of residual coupling and diminished effectiveness of the chromatic correction, as well as directly from the larger total emittance.

In these studies it was assumed that the first-order demagnification should be set as for the design input beam. In the next section we examine this question in detail.

4. OPTIMUM DEMAGNIFICATION

The demagnification can be characterized by the beta-function, β^* , at the IP. Assuming linear optics, the luminosity scales as $1/\beta^*$. At small values of β^* this linear approximation breaks down because of chromatic and geometric aberrations. Their dominating contributions are induced by first-order chromaticity and correctable within the FFS in a dedicated Chromatic Correction Section.¹⁰ The effective β^* due to the remaining higher order terms then becomes (see Ref. 5):

$$\beta_{eff}^* \approx \beta^* + \kappa_1^2 \frac{\delta_E^4}{\beta^*} + \kappa_2^2 \frac{\epsilon \delta_E^2}{\beta^{*2}} + \kappa_3^2 \frac{\epsilon^2}{\beta^{*3}} \quad , \quad (1)$$

where δ_E is the beam energy spread and $\kappa_1, \kappa_2, \kappa_3$ are measures of the residual second-order chromatic and geometric aberrations. The optimal demagnification, defined by minimal β_{eff}^* in Eq. (1), has been determined theoretically for a perfect beamline and is expected to be $\approx 4 \text{ mm}$.¹¹

Operationally, the demagnification is adjusted with the use of an online modeling and fitting package.⁷ After tuning the beams initially at $\beta^* \approx 3 \text{ cm}$ (where aberrations are small) the package infers the beam σ matrix at the entrance of the FFS from the measured beam parameters at the IP using a linear optics approach. New magnet settings are then determined to reach a desired smaller β_{des}^* at the IP. Besides being a strictly linear approach, the procedure is based on the assumptions that

the initial tuning at $\beta^* \approx 3$ cm was perfect and that the σ matrix at the IP is fully diagonal. As discussed above, the latter assumption will, in general, not be correct in the non-nominal case of unequal horizontal and vertical emittances (ϵ_x, ϵ_y), where two of the four cross-plane coupling terms cannot be controlled and corrected within the FFS.⁷

We used the interactive simulation package to study the stability of these matching procedures and determine the optimal demagnification under realistic conditions, taking the previously described arc matrices with random imperfections. Figure 4 summarizes the results of three typical examples. Shown are measured spot sizes $\sigma^* = (\sigma_x^* \cdot \sigma_y^*)^{1/2}$, the effective $\beta_{eff,x,y}^* = \sigma_{x,y}^* / \sigma_{x',y'}^*$, normalized to the desired β_{des}^* , and the apparent emittances $\epsilon_{eff,x,y}^* = \sigma_{x,y}^* \cdot \sigma_{x',y'}^*$, as functions of β_{des}^* . The initial setup corresponds to a well-tuned configuration with $\beta^* = 3$ cm. The new magnet settings for each β_{des}^* are determined as in the online β -matching algorithm described above. For each new β_{des}^* value the beam is returned at the IP.

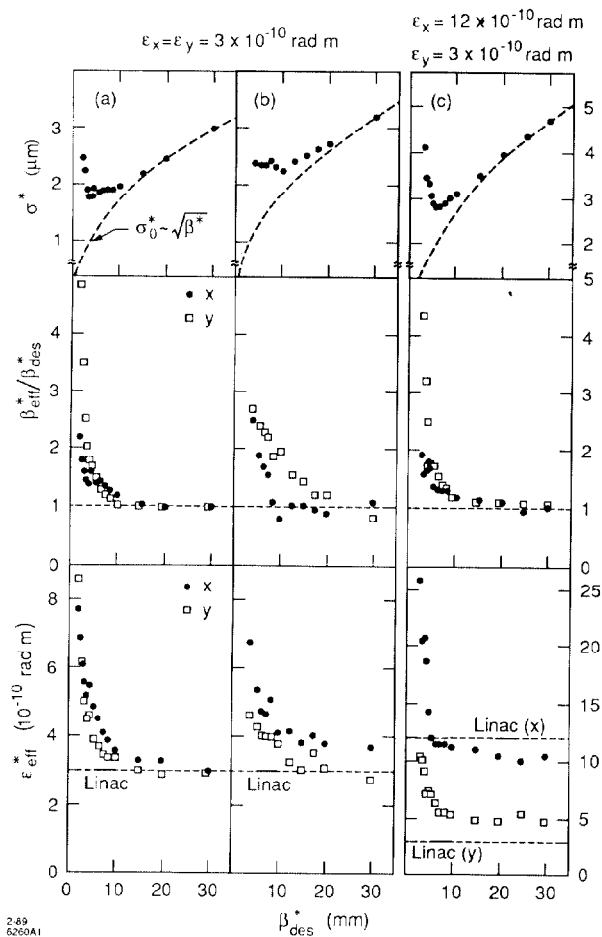


Fig. 4. IP spot size, ratio of effective to first-order β^* , and measured effective emittance as functions of the target value of β^* , for three examples: (a) and (b) nominal linac emittance with different random seeds for simulation of arc misalignment, and (c) larger linac emittance in one plane.

Figure 4(a) shows a random seed for which the results are close to the theoretical predictions for perfect conditions. The spot size decreases to well below $2 \mu\text{m}$ and the optimal β_{des}^* is

≈ 4 mm. For $\beta_{des}^* < 4$ mm the spot size increases drastically because of aberrations. Nonlinear effects start to be visible around $\beta_{des}^* \approx 15$ mm. Above this value first order beam parameters can be well measured.

The results of Fig. 4(b) originate from a random seed that leads to particularly large deviations from expectations for perfect conditions. Spot sizes drop to $\approx 2.5 \mu\text{m}$ at $\beta_{des}^* \approx 10$ mm. No clear minimum can be observed in this case. The vertical $\beta_{eff,y}^*$ starts to deviate from linear optics predictions already at $\beta_{des}^* \approx 20$ mm. The emittances at $\beta^* = 3$ cm are not identical to the input emittances which indicates cross-plane coupling effects due to the lattice errors in the arc.

A case of unequal horizontal and vertical emittances is shown in Fig. 4(c). The spot size reaches a minimum below $3 \mu\text{m}$ around $\beta_{des}^* \approx 6$ mm. Cross-plane coupling is more serious in this case because of the large horizontal emittance: The vertical emittance at $\beta^* = 3$ cm is $5 \cdot 10^{-10}$ rad-m which indicates a blowup of ϵ_y by 70% in the arc. The effective β_{eff}^* starts to deviate significantly from β_{des}^* at $\beta_{des}^* \approx 10$ mm.

In conclusion, for most of the studied scenarios the highest luminosity is reached at β^* values larger than the idealized theoretical prediction of 4 mm. Considering the sharp decrease of luminosity at β_{des}^* below the optimum, a value of $\beta_{des}^* \geq 6$ mm seems to be most appropriate operationally.

ACKNOWLEDGMENTS

Two of us (W. T. F. and T. L.) were supported, respectively, by a Faculty Fellowship from the University of Colorado and by a grant from the Max Kade Foundation.

REFERENCES

1. K. L. Brown, D. C. Carey, F. C. Iselin, and F. Rothacker, SLAC-Report-91 (Rev. 1973), NAL 91 and CERN 80-04 (1980).
2. D. C. Carey *et al.*, Slac-0246 (1982).
3. R. V. Servranckx *et al.*, SLAC Report 285, UC-28 (A) (1985).
4. D. C. Carey and F. C. Iselin, *Proc. of the 1984 Summer Study on the Design and Utilization of the Superconducting Super Collider*, Snowmass, CO, June 1984; D. Douglas, L. Healy, F. C. Iselin, and R. Ryne, SSC Aperture Workshop Summary, SSC-TR-2001, Appendix 7 (1984); F. C. Iselin, *The Mad Program Reference Manual*, CERN, LEP Division (1984).
5. P. Bambade, D. Burke, W. Kozanecki, T. Lohse, T. Mattison, N. Phinney, D. Ritson, W. Ford, C. Hawkes, W. Koska, and P. Burchat, *Operational Experience with Optical Matching in the SLC Final Focus System*, paper Q31 at this conference.
6. Karl L. Brown, private communication.
7. C. M. Hawkes and P. S. Bambade, *Nucl. Instr. and Meth.* **A274**(1989), 27.
8. The arc studies were performed by T. Fieguth.
9. P. S. Bambade, *Number of Dimensions of Optical Correction Space in the SLC Final Focus System*, collider note in preparation.
10. K. L. Brown, *A Conceptual Design of Final Focus Systems for Linear Colliders* SLAC-PUB-4227 (June 1987).
11. P. S. Bambade, *Beam Dynamics in the SLC Final Focus System*, SLAC-PUB-4227 (June 1987).